Work Function Modification in P3HT H/J Aggregate Nanostructures Revealed by Kelvin Probe Force Microscopy and Photoluminescence Imaging

Mina Baghgar[†,§] and Michael D. Barnes[*,†,‡]

[†]Department of Physics and [‡]Department of Chemistry, University of Massachusetts, Amherst, Massachusetts 01003, United States. [§]Present address: Department of Physics, Harvard University, 17 Oxford Street, Cambridge, Massachusetts 02138, United States.

ABSTRACT We show that surface electronic properties of poly-3-hexylthiophene (P3HT) crystalline nanofibers as probed by Kelvin probe force microscopy (KPFM) depends sensitively on the degree of polymer packing order and dominant coupling type (*e.g.*, H- or J-aggregate) as signaled by absorption or photoluminescence spectroscopy. Nominal HOMO energies between high molecular weight (J-aggregate) nanofibers and low-molecular weight (H-aggregate) nanofibers differ by ≈160 meV. This is consistent with shifts expected from H-type charge-transfer (CT) interactions that lower HOMO energies according to registration between thiophene moieties on adjacent polymer chains. These results show how KPFM combined with wavelength-resolved photoluminescence imaging can be used to extract information on "dark" (CT) interactions in polymer assemblies.

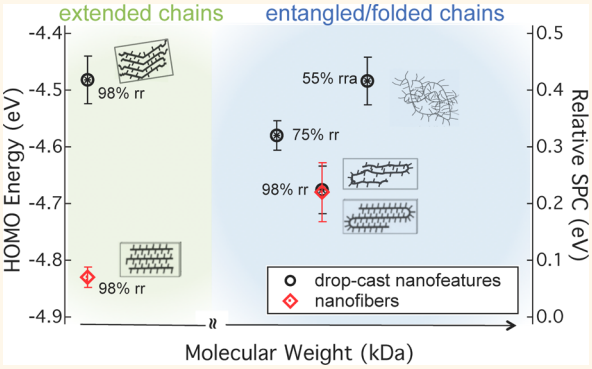

KEYWORDS: Kelvin probe force microscopy · photoluminescence · poly-3-hexylthiophene · P3HT · H/J aggregates · nanowires · interchain coupling

Since the discovery of crystalline nanofibers of semiconducting polymers (*e.g.*, poly-3-hexyl thiophene, P3HT),[1−3] there has been significant interest in optoelectronic applications of these preformed nanostructures.[4−9] Formed by self-assembly in marginal solvents, nanofibers are nominally formed by π-stacking of lamellar sheets, thus offering a fairly broad range of interchain order depending on intrinsic factors such as molecular weight and regioregularity, and solvent processing conditions.[8,10,11] Typically, the degree of interchain order is inferred from spectroscopic measurement of intensity ratios of the 0−0 and 0−1 vibronic peaks in either photoluminescence or absorption: Within the coupled Frenkel exciton (FE) model developed by Spano, dominant interchain coupling (associated with a high degree of interchain order) leads to H-type aggregate signatures with $I_{00}/I_{01} < 1$, while dominant intrachain coupling leads to J-type aggregates with $I_{00}/I_{01} \geq 1$. Recently, Spano and Yamagata proposed that charge-transfer (CT) interactions augment the usual coupled dipole model in a way that is highly sensitive to the registration between chromophores on adjacent chains, leading to so-called hybrid HJ coupling.[12] The charge-transfer interaction modulates the hole-transfer integral (related to energy shifts of the highest occupied molecular orbital) according to the spatial registration between adjacent chains. Such shifts—either positive or negative, depending on the degree of slip-stacking—would be impossible to observe directly by photoluminescence alone.

In this paper, we demonstrate significant variation in HOMO energies of nanofibrillar structures of P3HT with varying molecular weight and regioregularity as interrogated by Kelvin probe force microscopy (KPFM). The most dramatic effect is observed in comparing surface potential contrast (SPC)

* Address correspondence to mdbarnes@chem.umass.edu.

Received for review March 20, 2015 and accepted June 20, 2015.

Published online June 21, 2015
10.1021/acsnano.5b03422

of preformed crystalline nanofibers of low-molecular weight (13 kDa) P3HT with nanofibrillar structures of the same polymer formed by spontaneous dewetting of drop-cast solution; the photoluminescence spectra of the two species are very similar indicating H-type aggregation, yet differ in SPC by more than 300 meV. In contrast, comparison of SPC from crystalline nanofibers and drop-cast nanofibrils from higher molecular weight P3HT (65 kDa) shows virtually no change. We interpret these results in terms of the Spano HJ aggregate model in which the charge-transfer interaction for P3HT aggregates with a high degree of interchain order is predicted to lead to a lowering of the HOMO level.[12] These results, particularly for the low-molecular weight P3HT systems, are consistent with a positive H-like charge-transfer interaction that lowers the HOMO level with increasing π-stacking registration (stacking order). These results illustrate nicely the influence of interchain order on electronic properties in P3HT assemblies, and validate the predicted H-type charge-transfer interaction in this particular system. By combining photoluminescence with KPFM imaging, we are able to reveal new details on the connection between supramolecular structure and the influence of stacking disorder on electronic properties.

While there is an extensive literature on photoluminescence probes of P3HT aggregate structure[13] in films,[14,15] nanoparticles,[16−21] and nanofibers,[8,10] there is relatively limited experimental information on electronic properties correlated with different aggregate motifs with distinct H- or J-, or H/J coupled systems.[22,23] Liscio and co-workers used KPFM to probe charge transport in graphene-P3HT blends,[24,25]as well as nanofiber-like structures formed from dewetted P3HT films cast from chloroform,[26] to probe the modification of graphene electronic properties as influenced by P3HT additives. Ginger and co-workers have used both Kelvin probe and time-resolved electric force imaging techniques to probe the connection between electronic properties and local polymer morphology in solar cells,[27−29] and photoinduced charge transport.[30] The HOMO energy level of P3HT has been estimated to range between −5.2 and −4.8 eV from the space charge limited current (SCLC) analysis of hole-only thin film devices,[31] cyclic voltammetry,[32] photoelectron microscopy,[33] ultraviolet and (angle-resolved) X-ray photoelectron spectroscopy (UPS and AR-XPS),[34] and Kelvin probe force microscopy under either vacuum or ambient conditions.[26,35−37] This wide range of experimentally determined HOMO values of P3HT is attributed to the variation in the molecular packing of the polymer, which crucially depends on polymer properties and processing conditions. The HOMO value of P3HT thin films as probed by KPFM was shown to be highly sensitive to regioregularity, molecular weight, and film processing conditions such as annealing temperature, and spin-cast rate.[34]

Moreover, KPFM study on the P3HT-*b*-P3MT nanofibers revealed that HOMO energy of aggregates could be further tuned by varying polymer chain order in preformed nanostructures.[38,39]

Recent work in our laboratory has shown how photoluminescence probes of nanofibers made with P3HT of varying molecular weight provided new insights on how molecular packing and polymer chain conformation affect aggregate structure.[11,40] In P3HT nanowire assemblies, a (negative) through-bond Frenkel exciton (FE) coupling along the polymer chain combined with a (positive) through-space interchain charge-transfer interaction leads to a hybrid aggregate type with spectroscopic characteristics of both "H-type" (charge-transfer) and "J-type" (FE coupling) aggregates.[12] More recently, a similar analysis of combined FE and CT coupling in tetra-aza-terrylene (TAT) single crystals showed the fascinating property that the sign of these interactions can be reversed depending on the specific packing geometry of the molecules, leading to new design paradigms for organic electronic materials.[41] The tunability in both FE and CT interactions can lead to a spectrum of hybrid couplings (HH, HJ, JH, or JJ), suggesting the exciting possibility of strongly enhanced through-space exciton coupling facilitated by constructive interference of FE and CT coupling modes.[42] The experiments we report here are designed specifically to probe "dark" (CT) interactions independent of optical excitation.

RESULTS AND DISCUSSION

Figure 1 shows photoluminescence (PL) images of extended nanofibrillar structures made from P3HT of different molecular weights and regioregularities: (a) 55% rra and 75 kDa, (b) 75% rr and 55 kDa, (c) 98% rr and 65 kDa, and (d) 98% rr and 13 kDa. These nanostructures were made from dewetting of highly diluted P3HT solution in chloroform (about 5 mg L^{-1}) drop cast on cover glass. The topography and surface potential of the structures are represented next to their corresponding PL images in Figure 1. Similar to the observations of Liscio and co-workers on studying spun-cast P3HT films,[26] we observed a network of fibrillar "nanowire" structures with almost uniform lateral size in high molecular weight (MW) drop-cast films with 55% (e) and 75% (f) regioregularity. However, drop casting high regioregular P3HT with either high MW (g) or low MW (h) resulted in nanofeatures with various lateral sizes. Scale bar in each KPFM images (i, j, k, l) denotes the surface potential contrast (SPC) of nanostructures relative to the floating cover glass.

Figure 2a and b represent the 2D scatter plots of drop-cast nanofeatures with different regioregularities, and drop-cast nanofeatures with different MWs, respectively. The drop-cast film with high MW and 98% regioregularity (black square) has a significantly broad height distribution compared to the other three films.

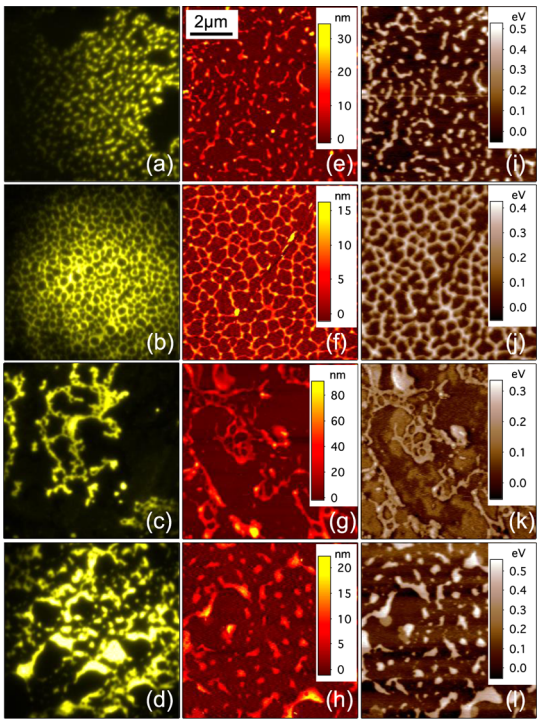

Figure 1. Photoluminescence images of fibrillar P3HT nanostructures from drop-cast chloroform solution on cover glass with (a) 55% rra and 75 kDa MW, (b) 75% rr and 55 kDa MW, (c) 98% rr and 65 kDa MW, (d) 98% rr and 13 kDa MW. The corresponding topography (e, f, g, h) and surface potential (i, j, k, l) of the nanostructures are shown on their right side of the PL images.

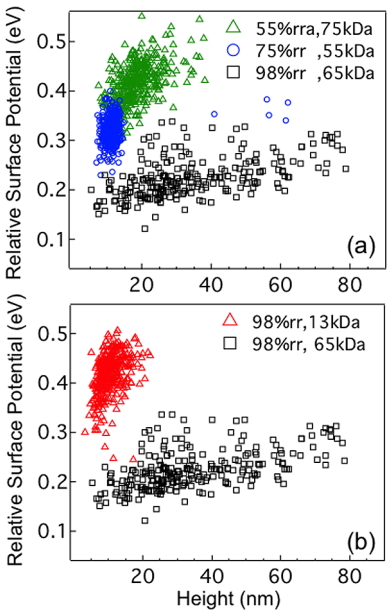

Figure 2. Scatter plot of measured relative SPC values of drop-cast nanostructures with (a) high molecular weight and different regioregularities (55% rra: green triangle, 75% rr: blue circle, and 98% rr: black square), and (b) different molecular weights (13 kDa: red triangle, and 65 kDa: black square) and high regioregularity.

However, mapping surface potential contrast of the corresponding nanostructures indicates a small variation in the SPC value with the shape and height of nanostructures within each family.

Figure 3a shows sampled photoluminescence spectra of the nanofibrillar P3HT structures corresponding to Figure 1. Note that the fibrillar structures generated from drop-cast high MW P3HT (55% rra: green line, 75% rr: blue line, 98% rr: black line) have broad PL spectra with no distinguishable vibronic features. In fact, these spectra closely resemble PL spectrum of amorphous P3HT in chloroform,[46] suggesting that these "nanowire" structures and possibly those interrogated in ref 26 are formed from spontaneous film dewetting, rather than crystalline self-assembly. The amorphous (largely disordered) characteristic of these nanostructures, broad PL spectrum peaked at 580 nm, reveals entangled conformation of their long polymer chains,[47,48] which leads to very weak exciton coupling between molecules in high MW nanowires. On the other hand, the PL spectrum of low MW drop-cast nanowires (red line) manifests crystalline aggregate characteristics with a red-shifted origin compared to its high MW counterparts, and some (weak) vibronic structures. Its broad vibronic transition bandwidth is typical of strong disorder in the low MW nanowire structures. Also, it indicates that short chains are not entangled[47] but loosely packed in lamellae leading to the semicrystalline morphology of the drop-cast low MW nanowires.

Figure 3b shows that the average SPC of the nanofibrillar P3HT (from drop-cast solution) is strongly sensitive to both regioregularity and molecular weight. This is despite rather identical wavelength-resolved photoluminescence signature of high MW P3HT nanofeatures with random, low, and high regioregularities. The average SPC of amorphous nanowires relative to glass decreases from 0.41 to 0.22 eV as regioregularity of long chains increases from 55% (rra) to 98% (high-rr). The HOMO energy level of nanostructures can be calculated by subtracting the work function of the kelvin probe tip from the absolute SPC value ($SPC_{absolute} = SPC_{relative} + SPC_{glass}$), $HOMO = SP_{absolute} - WF_{tip}$. Therefore, the observed decrease in the relative SPC value with increasing regioregularity is associated with a decrease in HOMO energy level of high-rr amorphous nanofeatures. Since amorphous nanofeatures with different regioregularities show similar PL spectra, one would conclude that the observed shift in HOMO energy level induced by the enhanced regioregularity might be attributed to subtle differences in the structural order of amorphous nanofeatures that are not manifested in their optical properties.

Regiorandom chains (half-random mixed with head-to-head and head-to-tail) tend to irregularly pack and suffer a large torsional disorder with interchain spacing of about 4–4.5 Å measured from wide-angle X-ray diffraction patterns at room temperature.[5,48]

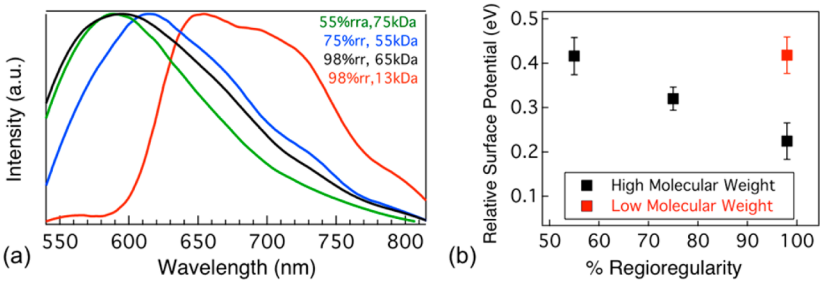

Figure 3. (a) PL spectra of P3HT nanostructures with different regioregularities and molecular weights: 55% rra and 75 kDa (green line), 75% rr and 55 kDa (blue line), 98% rr and 65 kDa (black line), and 98% rr and 13 kDa (red line). (b) The corresponding averaged measured surface potential of nanostructure in (a), relative to cover glass, as a function of regioregularity. The black and red squares denote the high and low molecular weights, respectively.

Increasing regioregularity improves self-organization of chains by keeping chains backbone within the lamellar sheets *via* $\pi-\pi$ stacking. This results in lower interchain spacing of high-rr nanowires, 3.8 Å, compared with rra-structures.[1] Reduced interchain spacing at high-rr nanofeatures enhances wave function overlap, which raise the rate at which charges move from site to site, so-called charge-transfer integral. This increases ionization energy measured *via* UPS and AR-XPS methods,[34] equivalent to the observed reduced HOMO energy level. However, the variation in interchain spacing might not be sufficient to recover the excitonic coupling in the amorphous nanostructures. On the other hand, decreasing molecular weight of high-rr polymer from 65 to 13 kDa *increases* the relative SPC value from 0.22 to 0.41 eV (red squares in Figure 3b). This rather unintuitive observation of elevated HOMO energy level in high-rr semicrystalline nanostructures is accompanied by an increase in structural order evidenced by PL spectrum with emission origin at 640 nm, red line in Figure 3a. The enhanced HOMO energy level is accompanied and so could be attributed to an alternation in the chain conformation from strongly disentangled chains, in high-MW amorphous nanofeatures, to configuration in which each chains comprise of one or several planarized segments separated by additional coiled segments.[49] The striking changes in the HOMO of amorphous and semicrystalline nanofeatures with molecular weight suggests that chain conformation is a decisive factor in determining and tuning not only the strength of exciton coupling[11] but also the frontier energy level of the aggregates.

To further understand how chain conformation in nanostructures affects the HOMO energy level of P3HT aggregates, we examined electrical properties of two extreme cases: low-MW crystalline nanofibers with extended chain conformation and high-MW crystalline nanofibers with fully folded conformation. Relative orientation of the neighboring chains in P3HT aggregates identifies two types of configurations: head-to-tail structures (J-aggregate) and face-to-face structures (H-aggregate) that favor intrachain and interchain

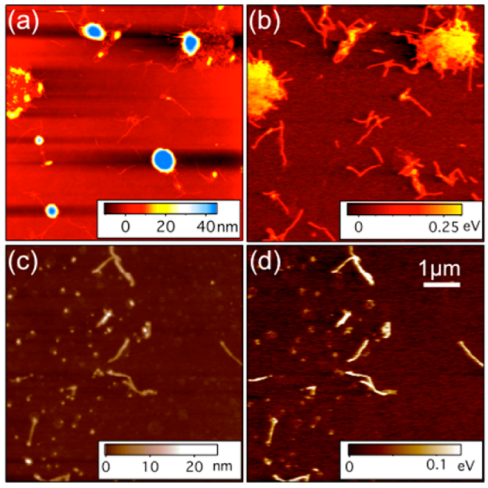

Figure 4. Height and surface potential images of high molecular weight (65 kDa) nanofibers (a, b) and low molecular weight (13 kDa) nanofibers (c,d) cast on cover glass. The average measured SPC for 65 and 13 kDa nanofibers are 200 and 65 meV, respectively, relative to cover glass. Features with height above 30 nm in (a) and small diameters in (c) have amorphous PL characteristic with average zero relative SPC value shown in (b).

exciton couplings, respectively.[23,50] In the recent size correlated PL spectroscopy study on P3HT nanofibers,[11] we showed that the polymer chain folding within the lamellae induces a transition from H-aggregate to J-aggregate and thus reduces effective dimensionality of exciton coupling within the crystalline nanofibers from 2D (both inter- and intrachain coupling) to 1D (almost exclusively intrachain coupling).[11] Comparison of SPC values of nanofibers with high and low MW could then indicate the extent to which the variation in crystalline order and the dominant aggregate structure (H- *vs* J-aggregate) affects HOMO energy level. Figure 4 shows height and surface potential images of well-separated high-rr crystalline nanofibers with 13 kDa and 65 kDa MW that are cast on piranha-treated cover glass. The KPFM images (b and d) indicate lower relative SPC value (0.06 ± 0.02 eV) for low-MW crystalline nanofibers (d) as compared with high-MW crystalline nanofibers with relative SPC value of 0.22 ± 0.05 eV (b). The

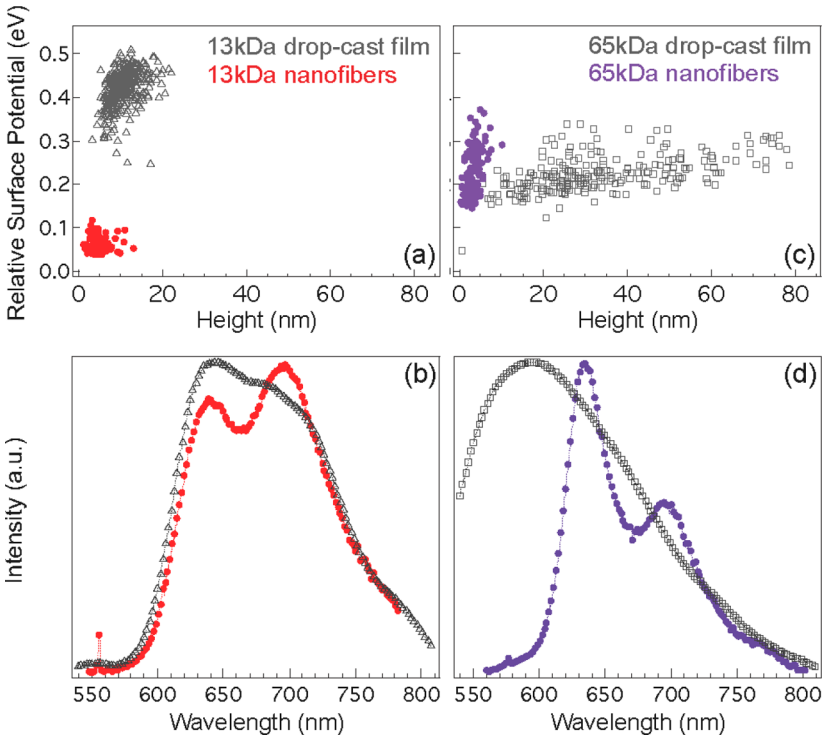

Figure 5. Two-dimensional scatter plot of surface potential of low (a) and high (c) molecular weight P3HT nanofibers and drop-cast nanowires and their height. In both graphs gray markers are drop-cast nanowires and colored markers are crystalline nanofibers. (b, d) The corresponding PL spectra of drop-cast nanofeatures and crystalline nanofibers with low and high molecular weights, respectively.

average width of 13 kDa and 65 kDa crystalline NFs are 14 and 17 nm, respectively, measured from the TEM images.[11] It is well-known that tip convolution in SPM is important when the lateral size of the scanned object is comparable to the tip diameter.[51] The measured surface potential of nanostructures in noncontact KPFM is a weighted average over so-called an effective area of the surface that is interacting with the tip through long-range electrostatic field. Thus, the kelvin probe signal is a linear convolution of an effective surface potential and microscope point spread function. The point-spread function can be calculated based on measuring the tip shape. Different deconvolution methods have been developed to reconstruct the KPFM images aiming to restore the actual SPC value of the nanostructures.[26,52−54] We realized that deconvolving the KPFM images in Figure 4b and d will only change the relative SPC value of NFs from 5 to 10%, depending on their height, within each family. Therefore, the observed difference in the average relative SP value of about 160 meV between 13 kDa and 65 kDa crystalline nanofibers is a real material property and not associated with convolution of the SPC signal with the underlying substrate.

Figure 5a represents 2D scatter plot of the relative surface potential contrast of 13 kDa self-assembled nanofibers and 13 kDa drop-cast nanowires. The surface potential of self-assembled nanofibers (red circles) has a narrow distribution with average value of 0.066 eV that is about 350 meV smaller than that of its counterpart (gray triangle). In addition, the PL spectra in Figure 5b show that self-assembled nanofibers have higher molecular order and stronger interchain coupling relative to drop-cast nanostructures evidenced by a decreased in the 0−0 to 0−1 PL intensity ratio from 1.12 to 0.9, and narrower vibronic transition bandwidth. Both low MW nanostructures possess extended chain conformation in lamellar sheets with dominant H-type aggregates. However, fibrilizing 13 kDa polymer chains in chloroform/DCM mixed solvent under thermal equilibrium condition results in higher chain planarization, superior molecular order, and thus stronger interchain coupling as compared with drop-cast nanowires in which aggregation is driven by solvent evaporation. This suggests that in the low molecular weight regime modifying molecular packing order might recover thiophene ring registration in adjacent lamellae and thus develop intermolecular charge distribution. This expands wave function overlap between the frontier orbitals leading to lower HOMO energy level.

Figure 5c shows 2D scatter plot of relative SPC of 65 kDa crystalline nanofibers, formed from CF/DCM mixed solvents (purple circle), and 65 kDa amorphous nanofeatures (gray square). The scatter plot shows almost similar average relative SPC value for the 65 kDa crystalline nanofibers and 65 kDa amorphous

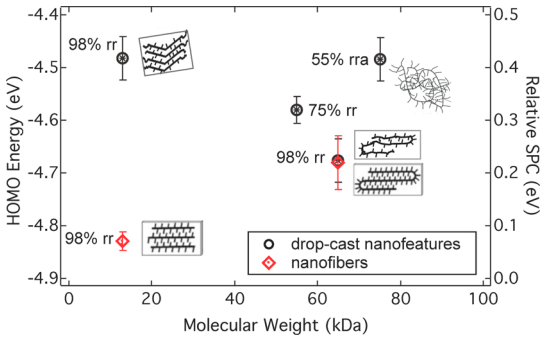

Figure 6. Schematic energy level diagram of the extended P3HT nanostructures, which illustrates the effect of P3HT regioregularity and chain conformation on HOMO level of nanostructures in low and high molecular weight regions.

nanofeatures, 0.22 eV *vs* 0.224 eV despite their absolutely distinguishable spectral signature shown in Figure 5c. The self-assembled 65 kDa nanofibers possess folded chains in the lamellar sheets with high order of chain planarity and have dominant J-aggregate coupling,[11] whereas high-regioregular drop-cast nanofeatures have entangled chains with amorphous PL characteristics (Figure 5d). Both folded and entangled conformations possibly have weak thiophene ring registration (slip-stacking) in the subsequent π-stacked lamellae. Improved chain planarization in crystalline NFs compared with amorphous nanofeatures mostly develops charge transfer between frontier orbitals of neighboring thiophene rings in the same chain and regulates intramolecular charge distribution. This will strengthen intrachain exciton coupling, evidenced by large 0−0 to 0−1 PL intensity ratio and narrow transition bandwidth of 65 kDa nanofibers (Figure 5d), but interestingly seems not to have any noticeable effect on HOMO energy level of the nanostructures.

Figure 6 illustrates energy level diagram of extended crystalline nanofibers and drop-cast nanofeatures with different regioregularities in high and low molecular weight regimes. In low molecular weight regime, 13 kDa crystalline nanofibers have lower HOMO level than semicrystalline drop-cast 13 kDa nanofeatures. This considerable decrease in HOMO level is accompanied by stronger interchain exciton coupling in crystalline nanofibers (Figure 5c), suggesting that enhanced structural order and chain planarization mostly expand interchain charge distribution in the aggregates with extended chain conformation. In high molecular weight regime, HOMO level is inversely correlated with P3HT regioregularity. Increasing regioregularity essentially lessens interchain spacing by forcing entangled chains to pack into lamellae which enhances wave function overlap in the high molecular weight aggregates that show amorphous PL characteristics. However, HOMO energy levels of 65 kDa crystalline nanofibers and 65 kDa drop-cast nanofeatures with amorphous PL characteristics are almost similar implying that modifying chain planarization or lowering torsional disorder in the structure of high regioregular P3HT in this regime has a faint effect on the HOMO levels of the resultant structure. Correlating PL properties of nanostructures with their HOMO level indicates that the observed disparity in the correlation between morphology and electronic properties of high-rr P3HT aggregates in the two regimes (high and low MWs) is due to the difference in the chain conformation between the nanostructures. Interchain coupling within aggregates is almost very week, possibly due to thiophene ring misalignment between adjacent lamellar sheets in π-stacks. This miss-alignment is possible for both entangled and folded conformations of long chains. Therefore, improving molecular order in high-MW structures mostly enhances intramolecular charge distribution and intrachain exciton coupling but possibly do not affect interchain wave function overlap very much that appears to play a key role in electrical properties of the nanostructures.

CONCLUSIONS

KPFM measurements have revealed an interesting dependence of surface potential contrast (SPC) or HOMO energy level with P3HT interchain order. In comparing relative SPC value of P3HT nanostructures with different molecular weights and regioregularities, we found that the correlation between the amount of disorder present in the aggregate and electronic properties depend strongly on the chain conformation in the aggregates; for low molecular-weight crystalline nanofibers, the enhanced interchain order results in a dramatic decrease of the HOMO energy level with respect to the disordered drop-cast structures. This is consistent with an H-type charge-transfer interaction predicted for P3HT,[22] and also with the work of Stingelin, and co-workers,[55] on the low MWs paraffinic crystalline phase. We also observed that increasing regioregularity of high MW nanostructures with entangled chain conformation lowers their HOMO level. However, alternation in the chain planarization of high regioregular polymers in this regime induces subtle changes in the HOMO level of the resultant structure. The high MW regime is morphologically far more complex; in this regime there are also amorphous regions containing the elongated polymer chains that connect different domains. It is possible that the insensitivity of the SPC results to further chain planarization is due to an averaging over the smaller ordered regions (folded chains) and a larger amorphous region, where the nominal domain sizes ($\approx$ 5−10 nm) are small compared to the tip radius. It is also interesting to point out that different crystalline nanofiber types ("edge-on" *vs* "face-on") show strong differences in ionization energies due to intrinsic molecular dipoles, which could contri-

bute to the measured HOMO energy difference between low MW crystalline nanofibers and drop-cast nanofibrils.[56,57,22] These results show how combined photoluminescence and KPFM can be used to probe effects of structure and morphology that are not accessible by either means alone.

EXPERIMENTAL METHODS

In order to correlate photophysical properties of extended P3HT nanostructures with their size and local surface potential, we used cover glass as substrate to have optical access to nanostructures. A two-step cleaning treatment was performed on float-glass coverslips to remove both contamination and any possible stray charges off the substrate.[43] The coverslips were first soaked in piranha solution (a mixture of sulfuric acid (H_2SO_4) and hydrogen peroxide (H_2O_2) with 1:1 volume ratio), and rinsed with deionized water. In the second step, the coverslips were soaked in dilute aqueous sodium hydroxide solution (NaOH) for 1 min to neutralize residual acidity and remove any surface charge residues. The float glasses were then rinsed by deionized water and dried with air.

Self-assembled crystalline nanofibers[8] were obtained by addition of a poor solvent (dichloromethane (DCM)) to solvated P3HT in chloroform to a final v/v ratio of 1:7 $CHCl_3$:CH_2Cl_2 and leaving the solution in dark, undisturbed, for 24 h. Dilute suspensions of the preformed nanofibers were dispersed in 1:7 $CHCl_3$:CH_2Cl_2 mixed solvent and casted to clean coverslips for optical and KPFM interrogation. P3HT nanofibrillar structures (made from the same polymer samples) were formed by spontaneous dewetting from drop-cast dilute polymer solutions in chloroform on precleaned coverslips.

KPFM as implemented on an atomic force microscope platform is a scanning probe technique that measures the local attractive or repulsive force experienced by the tip whose sign and magnitude are approximately defined by the work-function difference between the probe (typically Pt-coated Silicon) and the sample.[44] Our measurements were performed on a MFP-3D Asylum with a 20 nm lift height that represented a compromise between both lateral resolution (which favor smaller lift heights), and other contributions to the surface potential contrast signal (*e.g.*, van der Waals forces) that are minimized at higher lift heights. We used Platinum Silicide probes and calibrated the tip work function (~5.5 eV) from KPFM on evaporated gold substrates. We also measured the average surface potential of floating cover glass to be about +0.6 eV (relative to Pt tip), which corresponds to work function value of 4.9 eV consistent with the UPS measurements.[45]

Conflict of Interest: The authors declare no competing financial interest.

Acknowledgment. Support from the U.S. Department of Energy Grant # DE-FG02-05ER15695 (Program Manager: Larry Rahn) is gratefully acknowledged. We also thank Prof. F. C. Spano for helpful comments.

REFERENCES AND NOTES

1. Kim, D. H.; Han, J. T.; Park, Y. D.; Jang, Y.; Cho, J. H.; Hwang, M.; Cho, K. Single-Crystal Polythiophene Microwires Grown by Self-Assembly. *Adv. Mater.* **2006**, *18*, 719–723.
2. Kim, D. H.; Jang, Y.; Park, Y. D.; Cho, K. Controlled One-Dimensional Nanostructures in Poly(3-Hexylthiophene) Thin Film for High-Performance Organic Field-Effect Transistors. *J. Phys. Chem. B* **2006**, *110*, 15763–15768.
3. Lim, J. A.; Liu, F.; Ferdous, S.; Muthukumar, M.; Briseno, A. L. Polymer Semiconductor Crystals. *Mater. Today* **2010**, *13*, 14–24.
4. Zhang, Y. J.; Dong, H. L.; Tang, Q. X.; Ferdous, S.; Liu, F.; Mannsfeld, S. C. B.; Hu, W. P.; Briseno, A. L. Organic Single-Crystalline p−n Junction Nanoribbons. *J. Am. Chem. Soc.* **2010**, *132*, 11580–11584.
5. Briseno, A. L.; Mannsfeld, S. C. B.; Shamberger, P. J.; Ohuchi, F. S.; Bao, Z. N.; Jenekhe, S. A.; Xia, Y. N. Self-Assembly, Molecular Packing, and Electron Transport in n-Type Polymer Semiconductor Nanobelts. *Chem. Mater.* **2008**, *20*, 4712–4719.
6. Briseno, A. L.; Kim, F. S.; Babel, A.; Xia, Y. N.; Jenekhe, S. A. n-Channel Polymer Thin Film Transistors With Long-Term Air-Stability And Durability and Their Use in Complementary Inverters. *J. Mater. Chem.* **2011**, *21*, 16461–16466.
7. Kamkar, D. A.; Wang, M. F.; Wudl, F.; Nguyen, T. Q. Single Nanowire OPV Properties of a Fullerene-Capped P3HT Dyad Investigated Using Conductive and Photoconductive AFM. *ACS Nano* **2012**, *6*, 1149–1157.
8. Baghgar, M.; Labastide, J.; Bokel, F.; Dujovne, I.; McKenna, A.; Barnes, A. M.; Pentzer, E.; Emrick, T.; Hayward, R.; Barnes, M. D. Probing Inter- and Intra-chain Exciton Coupling in Isolated Poly(3-hexylthiophene) Nanofibers: Effect of Solvation and Regioregularity. *J. Phys. Chem. Lett.* **2012**, *3*, 1674–1679.
9. Chou, C.-C.; Wu, H.-C.; Lin, C.-J.; Ghelichkhani, E.; Chen, W.-C. Morphology and Field-Effect Transistor Characteristics of Electrospun Nanofibers Prepared from Crystalline Poly-(3-hexylthiophene) and Polyacrylate Blends. *Macromol. Chem. Phys.* **2013**, *214*, 751–760.
10. Niles, E. T.; Roehling, J. D.; Yamagata, H.; Wise, A. J.; Spano, F. C.; Moule, A. J.; Grey, J. K. J-Aggregate Behavior in Poly-3-hexylthiophene Nanofibers. *J. Phys. Chem. Lett.* **2012**, *3*, 259–263.
11. Baghgar, M.; Labastide, J. A.; Bokel, F.; Hayward, R. C.; Barnes, M. D. Effect of Polymer Chain Folding on the Transition from H- to J-Aggregate Behavior in P3HT Nanofibers. *J. Phys. Chem. C* **2014**, *118*, 2229–2235.
12. Yamagata, H.; Pochas, C. M.; Spano, F. C. Designing J- and H-Aggregates through Wave Function Overlap Engineering: Applications to Poly(3-hexylthiophene). *J. Phys. Chem. B* **2012**, *116*, 14494–14503.
13. Barnes, M. D.; Baghar, M. Optical probes of chain packing structure and exciton dynamics in polythiophene films, composites, and nanostructures. *J. Polym. Sci., Part B: Polym. Phys.* **2012**, *50*, 1121–1129.
14. Clark, J.; Chang, J. F.; Spano, F. C.; Friend, R. H.; Silva, C. Determining Exciton Bandwidth And Film Microstructure In Polythiophene Films Using Linear Absorption Spectroscopy. *Appl. Phys. Lett.* **2009**, *94*, 163306.
15. Clark, J.; Silva, C.; Friend, R. H.; Spano, F. C. Role Of Intermolecular Coupling In The Photophysics Of Disordered Organic Semiconductors: Aggregate Emission In Regioregular Polythiophene. *Phys. Rev. Lett.* **2007**, *98*, 206406.
16. Labastide, J. A.; Baghgar, M.; Dujovne, I.; Yang, Y. P.; Dinsmore, A. D.; Sumpter, B. G.; Venkataraman, D.; Barnes, M. D. Polymer Nanoparticle Superlattices for Organic Photovoltaic Applications. *J. Phys. Chem. Lett.* **2011**, *2*, 3085–3091.
17. Labastide, J. A.; Baghgar, M.; Dujovne, I.; Venkatraman, B. H.; Ramsdell, D. C.; Venkataraman, D.; Barnes, M. D. Time- and Polarization-Resolved Photoluminescence of Individual Semicrystalline Polythiophene (P3HT) Nanoparticles. *J. Phys. Chem. Lett.* **2011**, *2*, 2089–2093.
18. Moule, A. J.; Allard, S.; Kronenberg, N. M.; Tsami, A.; Scherf, U.; Meerholz, K. Effect of Polymer Nanoparticle Formation On The Efficiency Of Polythiophene Based "Bulk-Heterojunction" Solar Cells. *J. Phys. Chem. C* **2008**, *112*, 12583–12589.
19. Nagarjuna, G.; Baghgar, M.; Labastide, J. A.; Algaier, D. D.; Barnes, M. D.; Venkataraman, D. Tuning Aggregation of Poly(3-hexylthiophene) within Nanoparticles. *ACS Nano* **2012**, *6*, 10750–10758.
20. Tenery, D.; Gesquiere, A. J. Interplay Between Fluorescence and Morphology in Composite MEH-PPV/PCBM Nanoparticles Studied at the Single Particle Level. *Chem. Phys.* **2009**, *365*, 138–143.

21. Vogelsang, J.; Adachi, T.; Brazard, J.; Bout, D. A. V.; Barbara, P. F. Self-Assembly of Highly Ordered Conjugated Polymer Aggregates with Long-Range Energy Transfer. *Nat. Mater.* **2011**, *10*, 942–946.
22. Fukuda, T.; Takagi, K.; Asano, T.; Honda, Z.; Kamata, N.; Shirai, H.; Ju, J.; Yamagata, Y.; Tajima, Y. Improved Power Conversion Efficiency of Organic Photovoltaic Cell Fabricated by Electrospray Deposition Method by Mixing Different Solvents. *Jpn. J. Appl. Phys., Part 1* **2012**, *51*, 02BK12.
23. Spano, F. C. The Spectral Signatures of Frenkel Polarons in H- and J-Aggregates. *Acc. Chem. Res.* **2010**, *43*, 429–439.
24. Liscio, A.; Palermo, V.; Samori, P. Nanoscale Quantitative Measurement of the Potential of Charged Nanostructures by Electrostatic and Kelvin Probe Force Microscopy: Unraveling Electronic Processes in Complex Materials. *Acc. Chem. Res.* **2010**, *43*, 541–550.
25. Liscio, A.; Veronese, G. P.; Treossi, E.; Suriano, F.; Rossella, F.; Bellani, V.; Rizzoli, R.; Samori, P.; Palermo, V. Charge Transport In Graphene-Polythiophene Blends As Studied By Kelvin Probe Force Microscopy And Transistor Characterization. *J. Mater. Chem.* **2011**, *21*, 2924–2931.
26. Liscio, A.; Palermo, V.; Samori, P. Probing Local Surface Potential of Quasi-One-Dimensional Systems: A KPFM Study Of P3HT Nanofibers. *Adv. Funct. Mater.* **2008**, *18*, 907–914.
27. Coffey, D. C.; Ginger, D. S. Time-Resolved Electrostatic Force Microscopy of Polymer Solar Cells. *Nat. Mater.* **2006**, *5*, 735–740.
28. Coffey, D. C.; Reid, O. G.; Rodovsky, D. B.; Bartholomew, G. P.; Ginger, D. S. Mapping Local Photocurrents in Polymer/Fullerene Solar Cells with Photoconductive Atomic Force Microscopy. *Nano Lett.* **2007**, *7*, 738–744.
29. Giridharagopal, R.; Shao, G. Z.; Groves, C.; Ginger, D. S. New SPM Techniques for Analyzing OPV Materials. *Mater. Today* **2010**, *13*, 50–56.
30. Noone, K. M.; Subramaniyan, S.; Zhang, Q.; Cao, G.; Jenekhe, S. A.; Ginger, D. S. Photoinduced Charge Transfer and Polaron Dynamics in Polymer and Hybrid Photovoltaic Thin Films: Organic *vs* Inorganic Acceptors. *J. Phys. Chem. C* **2011**, *115*, 24403–24410.
31. Chirvase, D.; Chiguvare, Z.; Knipper, M.; Parisi, J.; Dyakonov, V.; Hummelen, J. C. Electrical And Optical Design And Characterisation Of Regioregular Poly(3-Hexylthiophene-2,5diyl)/Fullerene-Based Heterojunction Polymer Solar Cells. *Synth. Met.* **2003**, *138*, 299–304.
32. Valaski, R.; Moreira, L. M.; Micaroni, L.; Hümmelgen, I. A. Charge Injection And Transport In Electrochemical Films Of Poly(3-Hexylthiophene). *J. Appl. Phys.* **2002**, *92*, 2035–2040.
33. Onoda, M.; Tada, K.; Zakhidov, A. A.; Yoshino, K. Photoinduced Charge Separation in Photovoltaic Cell with Heterojunction of p- And n-Type Conjugated Polymers. *Thin Solid Films* **1998**, *331*, 76–81.
34. Tsoi, W. C.; Spencer, S. J.; Yang, L.; Ballantyne, A. M.; Nicholson, P. G.; Turnbull, A.; Shard, A. G.; Murphy, C. E.; Bradley, D. D. C.; *et al.* Effect of Crystallization on the Electronic Energy Levels and Thin Film Morphology of P3HT:PCBM Blends. *Macromolecules* **2011**, *44*, 2944–2952.
35. Wu, M.-C.; Wu, Y.-J.; Yen, W.-C.; Lo, H.-H.; Lin, C.-F.; Su, W.-F. Correlation Between Nanoscale Surface Potential and Power Conversion Efficiency of P3HT/TiO_2 Nanorod Bulk Heterojunction Photovoltaic Devices. *Nanoscale* **2010**, *2*, 1448–1454.
36. Davis, R. J.; Lloyd, M. T.; Ferreira, S. R.; Bruzek, M. J.; Watkins, S. E.; Lindell, L.; Sehati, P.; Fahlman, M.; Anthony, J. E.; Hsu, J. W. P. Determination Of Energy Level Alignment at Interfaces of Hybrid and Organic Solar Cells Under Ambient Environment. *J. Mater. Chem.* **2011**, *21*, 1721–1729.
37. Xu, T.; Venkatesan, S.; Galipeau, D.; Qiao, Q. Study Of Polymer/ZnO Nanostructure Interfaces by Kelvin Probe Force Microscopy. *Sol. Energy Mater. Sol. Cells* **2013**, *108*, 246–251.
38. Baghgar, M.; Pentzer, E.; Wise, A. J.; Labastide, J. A.; Emrick, T.; Barnes, M. D. Cross-Linked Functionalized Poly(3-hexylthiophene) Nanofibers with Tunable Excitonic Coupling. *ACS Nano* **2013**, *7*, 8917–8923.
39. Baghgar, M.; Barnes, A. M.; Pentzer, E.; Wise, A. J.; Hammer, B. A. G.; Emrick, T.; Dinsmore, A. D.; Barnes, M. D. Morphology-Dependent Electronic Properties in Cross-Linked (P3HT-*b*-P3MT) Block Copolymer Nanostructures. *ACS Nano* **2014**, *8*, 8344–8349.
40. Baghgar, M.; Pentzer, E.; Wise, A. J.; Labastide, J. A.; Emrick, T.; Barnes, M. D. Cross-Linked Functionalized Poly(3-hexylthiophene) Nanofibers with Tunable Excitonic Coupling. *ACS Nano* **2013**, *7*, 8917–8923.
41. Yamagata, H.; Maxwell, D. S.; Fan, J.; Kittilstved, K. R.; Briseno, A. L.; Barnes, M. D.; Spano, F. C. HJ-Aggregate Behavior of Crystalline 7,8,15,16-Tetraazaterrylene: Introducing a New Design Paradigm for Organic Materials. *J. Phys. Chem. C* **2014**, *118*, 28842–28854.
42. Hestand, N. J.; Tempelaar, R.; Knoester, J.; Jansen, T. L. C.; Spano, F. C. Exciton Mobility Control Through sub-Å Packing Modifications in Molecular Crystals. *Phys. Rev. B: Condens. Matter Mater. Phys.* **2015**, *91*, 195315.
43. Yates, B. W.; Duffy, A. M. Statistical Analysis of the Metrological Properties of Float Glass. *Proc. SPIE* **2008**, 70770D–70770D-11.
44. Melitz, W.; Shen, J.; Kummel, A. C.; Lee, S. Kelvin Probe Force Microscopy and its Application. *Surf. Sci. Rep.* **2011**, *66*, 1–27.
45. Muray, J. J. Surface Conductivity of Borosilicate Glass. *J. Appl. Phys.* **1962**, *33*, 1527–1530.
46. Hu, Z.; Zou, J.; Deibel, C.; Gesquiere, A. J.; Zhai, L. Single-Molecule Spectroscopy and AFM Morphology Studies of a Diblock Copolymer Consisting of Poly(3-hexylthiophene) and Fullerene. *Macromol. Chem. Phys.* **2010**, *211*, 2416–2424.
47. Reid, O. G.; Malik, J. A. N.; Latini, G.; Dayal, S.; Kopidakis, N.; Silva, C.; Stingelin, N.; Rumbles, G. The Influence of Solid-State Microstructure on the Origin and Yield of Long-Lived Photogenerated Charge in Neat Semiconducting Polymers. *J. Polym. Sci., Part B: Polym. Phys.* **2012**, *50*, 27–37.
48. Shen, X.; Duzhko, V. V.; Russell, T. P. A Study on the Correlation Between Structure and Hole Transport in Semi-Crystalline Regioregular P3HT. *Adv. Energy Mater.* **2013**, *3*, 263–270.
49. Scharsich, C.; Lohwasser, R. H.; Sommer, M.; Asawapirom, U.; Scherf, U.; Thelakkat, M.; Neher, D.; Köhler, A. Control of Aggregate Formation in Poly(3-Hexylthiophene) by Solvent, Molecular Weight, and Synthetic Method. *J. Polym. Sci., Part B: Polym. Phys.* **2012**, *50*, 442–453.
50. Kasha, M. Energy Transfer Mechanisms and the Molecular Exciton Model for Molecular Aggregates. *Radiat. Res.* **2012**, *178*, AV27–AV34.
51. Samorí, P.; Francke, V.; Mangel, T.; Müllen, K.; Rabe, J. P. Poly-Para-Phenylene-Ethynylene Assemblies for a Potential Molecular Nanowire: An SFM Study. *Opt. Mater.* **1998**, *9*, 390–393.
52. Strassburg, E.; Boag, A.; Rosenwaks, Y. Reconstruction of Electrostatic Force Microscopy Images. *Rev. Sci. Instrum.* **2005**, *76*, 083705.
53. Machleidt, T.; Sparrer, E.; Kapusi, D.; Franke, K. H. Deconvolution of Kelvin Probe Force Microscopy Measurements—Methodology and Application. *Meas. Sci. Technol.* **2009**, *20*, 084017.
54. Jie, X.; Jun, X.; Yuefei, W.; Yunqing, C.; Wei, L.; Linwei, Y.; Kunji, C. Microscopic and Macroscopic Characterization of the Charging Effects in SiC/Si Nanocrystals/SiC Sandwiched Structures. *Nanotechnology* **2014**, *25*, 055703.
55. Koch, F. P. V.; Rivnay, J.; Foster, S.; Muller, C.; Downing, J. M.; Buchaca-Domingo, E.; Westacott, P.; Yu, L. Y.; Yuan, M. J.; Baklar, M.; *et al.* The Impact of Molecular Weight on Microstructure and Charge Transport in Semicrystalline Polymer Semiconductors Poly(3-Hexylthiophene), A Model Study. *Prog. Polym. Sci.* **2013**, *38*, 1978–1989.
56. Fabiano, S.; Yoshida, H.; Chen, Z.; Facchetti, A.; Loi, M. A. Orientation-Dependent Electronic Structures and Charge Transport Mechanisms in Ultrathin Polymeric n-Channel Field-Effect Transistors. *ACS Appl. Mater. Interfaces* **2013**, *5*, 4417–4422.
57. Heimel, G.; Salzmann, I.; Duhm, S.; Rabe, J. P.; Koch, N. Intrinsic Surface Dipoles Control the Energy Levels of Conjugated Polymers. *Adv. Funct. Mater.* **2009**, *19*, 3874–3879.